Applied and Computational Mechanics 7 (2013) 235–250

Applied and Computational Mechanics

Prediction of the nuclear fuel rod abrasion

V. Zeman[a,*], Z. Hlaváč[a]

[a] *Faculty of Applied Sciences, University of West Bohemia, Univerzitní 22, 306 14 Plzeň, Czech Republic*

Received 3 September 2013; received in revised form 2 December 2013

Abstract

The paper is focused on calculation of the friction forces work in the contact of nuclear fuel rods with fuel assembly spacer grid cells. This friction work is deciding factor for the prediction of the fuel rod coating abrasion. The fuel rod abrasion is caused by fuel assembly vibrations excited by pressure pulsations of the cooling liquid generated by main circulation pumps. A prediction of fuel rod coating abrasion makes use of experimentally investigated dependence of the abrasion on the friction force work in laboratory conditions. The presented original analytical-numerical method is applied for nuclear fuel rod inside of the Russian TVSA-T fuel assembly in the WWER 1000/320 type reactor core in NPP Temelín.

© 2013 University of West Bohemia. All rights reserved.

Keywords: vibrations, nuclear fuel assembly, pressure pulsations, dynamic load, fuel rod abrasion

1. Introduction

An assessment of nuclear fuel assemblies (FA) behaviour at standard operating conditions of the nuclear reactors belongs to important safety and reliability audits. A significant part of FA assessment plays abrasion of fuel rods coating [1].

The goal of this paper, in direct consequence of FA modelling in [7] and FA dynamic response excited by pressure pulsations presented in [5], is an introduction of the newly developed method for prediction of fuel rod abrasion caused by their flexural vibration. Elastic properties of the spacer grids between inner FA components are in the FA computational model expressed by alternate linear spring k_g centrally placed between fuel rods, guide thimbles and centre tube (see Fig. 1) on several vertical spacings $g = 1, \ldots, G$ [5, 7]. A real contact between inner fuel rods and spacer grids is realized by three cells $i = 1, 2, 3$ (see Fig. 2). Elastic properties of each cell can be expressed by three springs with identical stiffnesses k. The contact forces (in the picture $F_{u,i}$) between fuel rods (FR) and cells are deciding factor for the prediction of the FR abrasion.

The undermentioned method is focused on prediction of the FR abrasion caused by flexural FR vibrations in-spacer grids. FR vibrations are caused by spatial motion of the FA support plates in reactor core excited by pressure pulsations generated by main circulation pumps in the coolant loops of the reactor primary circuit [3]. Solution is based on knowledge of the spacer grid cell stiffnesses k calculated by FEM in ŠKODA JS [2] and experimentally investigated dependence of the FR abrasion on the friction force work in the contact line between FR laboratory sample and pressure plate [4].

*Corresponding author. Tel.: +420 377 632 332, e-mail: zemanv@kme.zcu.cz.

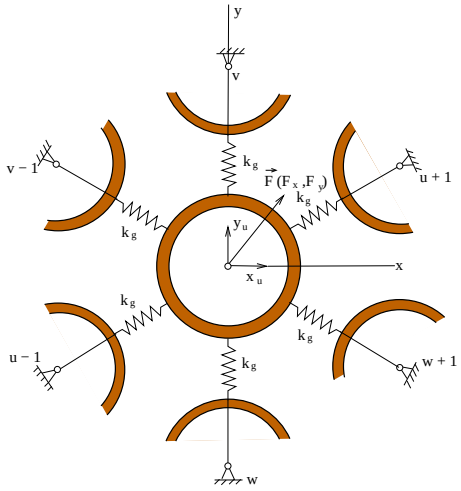

Fig. 1. The alternate couplings between fuel rods

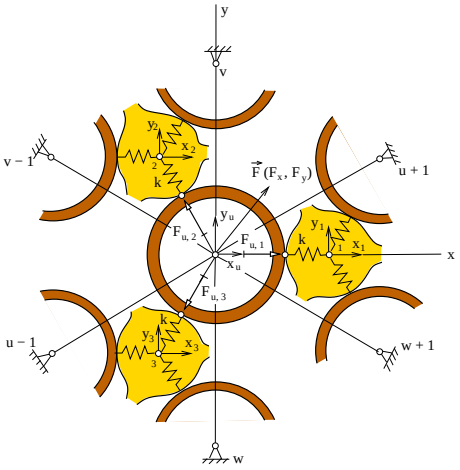

Fig. 2. The real couplings between fuel rods by means of cells

2. Shortly to computational and mathematical model of the nuclear fuel assembly

The FA basic structure is formed from large number of parallel identical fuel rods, some guide thimbles and centre tube. These FA components are linked by transverse spacer grids to each other and with skeleton construction (Fig. 3). The spacer grids are placed on several horizontal level spacings between support plates in reactor core (RC) as it is shown in the scheme of the reactor WWER 1000 in the Fig. 4.

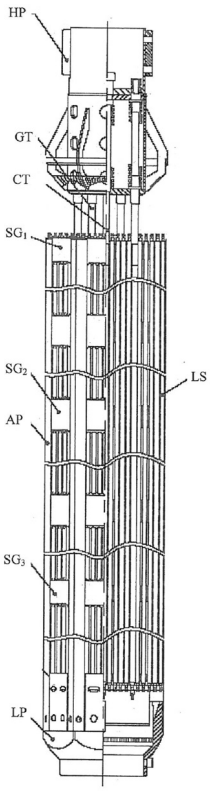

Fig. 3. Scheme of the fuel assembly

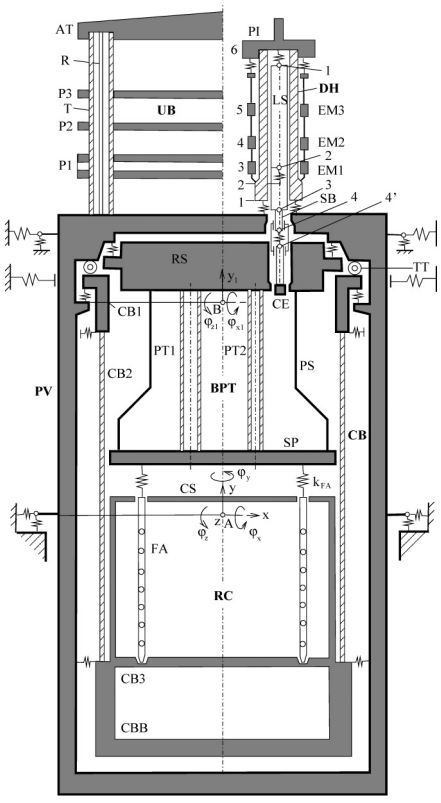

Fig. 4. Scheme of the reactor

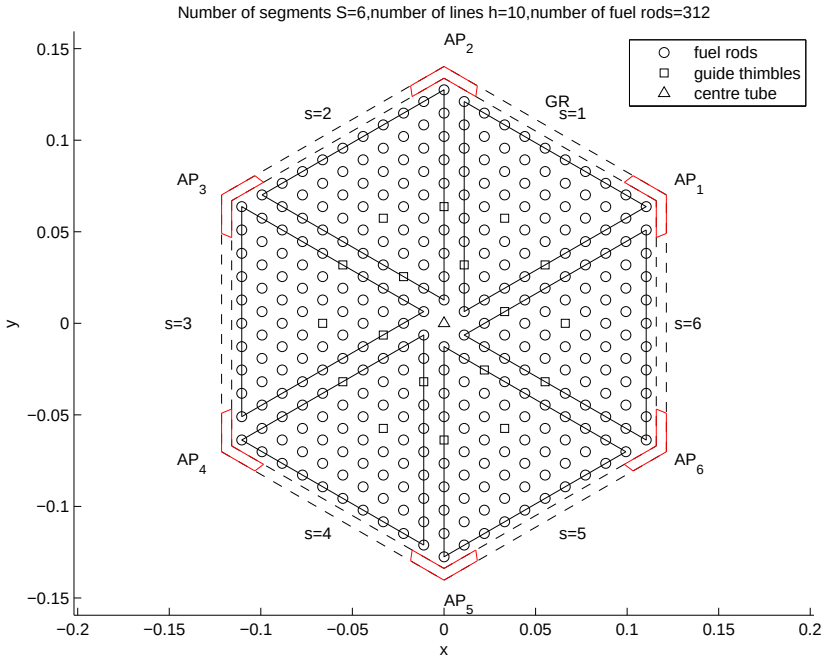

Fig. 5. The FA cross-section

In order to model the fuel assembly, the system is divided into subsystems – identical rod segments (S), centre tube (CT) and load-bearing skeleton (LS) fixed in bottom part in lower piece (Fig. 3). Because of the cyclic and central symmetric package of fuel rods and guide thimbles with respect to centre tube (Fig. 5), the FA decomposition to the identical rod segment $s = 1, \ldots, S$ (on the Fig. 5 for $S = 6$) shall be applied. Each *rod segment* is composed of R fuel rods with fixed bottom ends in lower piece (LP) and guide thimbles (GT) fully restrained in lower and head pieces (HP). The fuel rods and guide thimbles are linked by transverse spacer grids of three types ($\mathrm{SG}_1 - \mathrm{SG}_3$) inside the segments. Elastic properties of the spacer grids in the FA computational model are expressed by linear springs placed on several level spacings $g = 1, \ldots, G$ (see Fig. 1). The fuel rods are embedded into spacer grid cells with small initial radial tension which should not be negative during core operation.

The mathematical model of the rod segment s isolated from adjacent segments (without linkages between segments) was derived in the special coordinate system [7]

$$\boldsymbol{q}_s = [\boldsymbol{q}_{1,s}^T, \ldots, \boldsymbol{q}_{r,s}^T, \ldots, \boldsymbol{q}_{R,s}^T]^T, \tag{1}$$

where $\boldsymbol{q}_{r,s}$ is vector of nodal point displacements of one rod r (fuel rod or guide thimble) on the level of all spacer grids g in the form

$$\boldsymbol{q}_{r,s} = [\ldots, \xi_{r,g}^{(s)}, \eta_{r,g}^{(s)}, \vartheta_{r,g}^{(s)}, \psi_{r,g}^{(s)}, \ldots]^T, \quad r = 1, \ldots, R; \quad g = 1, \ldots, G. \tag{2}$$

Lateral displacements $\xi_{r,g}^{(s)}$, $\eta_{r,g}^{(s)}$ of the rod centres are mutually perpendicular whereas displacements $\xi_{r,g}^{(s)}$ are radial with respect to vertical central axis of FA. Displacements $\vartheta_{r,g}^{(s)}$, $\psi_{r,g}^{(s)}$ are bending angles of rod cross-section around lateral axes (see Fig. 6).

The fully restrained *centre tube* (see Fig. 3 and Fig. 5) is discretized into G nodal points on the level of spacer grids $g = 1, \ldots, G$ by means of $G + 1$ prismatic beam finite elements in the coordinate system

$$\boldsymbol{q}_{CT} = [\ldots, x_g, y_g, \vartheta_g, \psi_g, \ldots]^T, \quad g = 1, \ldots, G, \tag{3}$$

where lateral displacements x_g, y_g are oriented into axes x, y (Fig. 5).

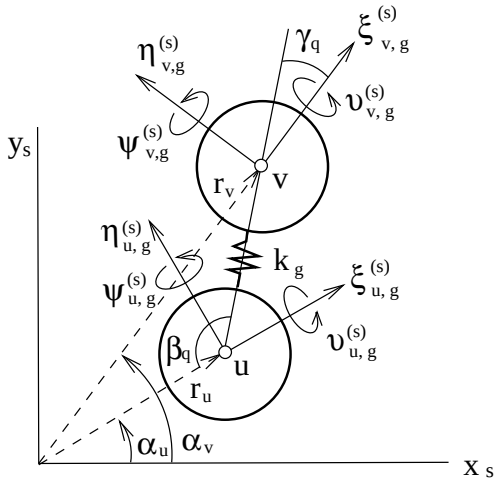

Fig. 6. The spring between two rods replacing the stiffness of spacer grid g

The *load-bearing skeleton* (further only skeleton) is created of S (on the Fig. 5 for $S = 6$) angle pieces (AP) coupled by divided grid rim (GR) at all levels of spacer grids. Each angle piece with fixed bottom ends in lower piece is discretized into nodal points in cross-section centre of gravity on the level of spacer grids $g = 1, \ldots, G$. The mathematical model of the skeleton without couplings with spacer grids is derived in the coordinate system

$$\boldsymbol{q}_{LS} = [\boldsymbol{q}_{AP_1}^T, \ldots, \boldsymbol{q}_{AP_s}^T, \ldots, \boldsymbol{q}_{AP_S}^T]^T, \tag{4}$$

where $\boldsymbol{q}_{AP_s}$ is vector of nodal points displacements for particular angle piece s on the level of all grid rim g in the form

$$\boldsymbol{q}_{AP_s} = [\ldots, \xi_{AP,g}^{(s)}, \eta_{AP,g}^{(s)}, \varphi_{AP,g}^{(s)}, \vartheta_{AP,g}^{(s)}, \psi_{AP,g}^{(s)}, \ldots]^T, \quad g = 1, \ldots, G. \tag{5}$$

Lateral displacements $\xi_{AP,g}^{(s)}$, $\eta_{AP,g}^{(s)}$ of cross-section centre of gravity on the level of spacer grid g are mutually perpendicular whereas displacement $\xi_{AP,g}^{(s)}$ is radial. Displacements $\varphi_{AP,g}^{(s)}$, $\vartheta_{AP,g}^{(s)}$, $\psi_{AP,g}^{(s)}$ are torsional and bending angles of angle piece cross-section around vertical and lateral axes (detailed to [7]).

The subsystems of FA are linked by spacer grids of different types for $g = 1$, $g = 2, \ldots, G - 1$ and $g = G$. Mathematical models of segments are identical in consequence of radial and orthogonal fuel rods and guide thimbles displacements. Therefore, the *conservative model of the fuel assembly* in configuration space

$$\boldsymbol{q} = [\boldsymbol{q}_1^T, \ldots, \boldsymbol{q}_s^T, \ldots, \boldsymbol{q}_S^T, \boldsymbol{q}_{CT}^T, \boldsymbol{q}_{LS}^T]^T \tag{6}$$

of dimension $n = 4GRS + 4G + 5GS$ can be written as

$$\boldsymbol{M}\ddot{\boldsymbol{q}} + (\boldsymbol{K} + \boldsymbol{K}_{S,S} + \boldsymbol{K}_{S,CT} + \boldsymbol{K}_{S,LS})\boldsymbol{q} = \boldsymbol{0}. \tag{7}$$

The symmetrical mass $\boldsymbol{M}$ and stiffness $\boldsymbol{K}$ matrices correspond to a fictive fuel assembly divided into mutually uncoupled subsystems. Therefore, these matrices are block diagonal

$$\boldsymbol{M} = \mathrm{diag}\,[\boldsymbol{M}_S, \ldots, \boldsymbol{M}_S, \boldsymbol{M}_{CT}, \boldsymbol{M}_{LS}],\ \boldsymbol{K} = \mathrm{diag}\,[\boldsymbol{K}_S^*, \ldots, \boldsymbol{K}_S^*, \boldsymbol{K}_{CT}, \boldsymbol{K}_{LS}], \tag{8}$$

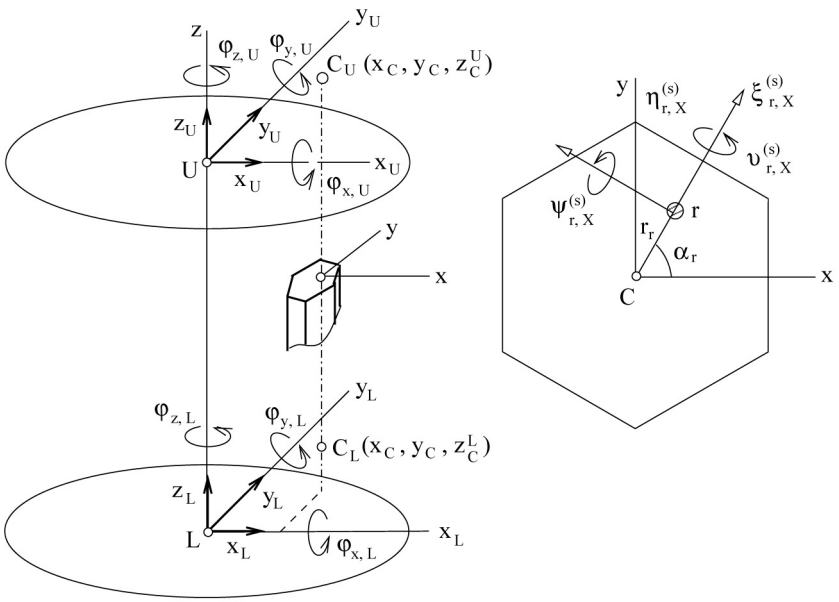

Fig. 7. Spatial motion of the FA support plates

where segment stiffness matrix $\boldsymbol{K}_S^*$ includes couplings between all fuel rods and guide thimbles inside the segment.

The coupling symmetrical stiffness matrices $\boldsymbol{K}_{SS}$, $\boldsymbol{K}_{S,CT}$ and $\boldsymbol{K}_{S,LS}$ express interaction between appropriate subsystems marked by subscripts. The stiffness matrix of all couplings between subsystems

$$\boldsymbol{K}_C = \boldsymbol{K}_{S,S} + \boldsymbol{K}_{S,CT} + \boldsymbol{K}_{S,LS} \tag{9}$$

has, for the hexagonal type FA ($S = 6$), block structure

$$\boldsymbol{K}_C = \begin{bmatrix} \boldsymbol{K}_{1,1} & \boldsymbol{K}_{1,2}^S & \boldsymbol{0} & \boldsymbol{0} & \boldsymbol{0} & \boldsymbol{K}_{1,6}^S & \boldsymbol{K}_{1,CT} & \boldsymbol{K}_{1,LS} \\ \boldsymbol{K}_{2,1}^S & \boldsymbol{K}_{2,2} & \boldsymbol{K}_{2,3}^S & \boldsymbol{0} & \boldsymbol{0} & \boldsymbol{0} & \boldsymbol{K}_{2,CT} & \boldsymbol{K}_{2,LS} \\ \boldsymbol{0} & \boldsymbol{K}_{3,2}^S & \boldsymbol{K}_{3,3} & \boldsymbol{K}_{3,4}^S & \boldsymbol{0} & \boldsymbol{0} & \boldsymbol{K}_{3,CT} & \boldsymbol{K}_{3,LS} \\ \boldsymbol{0} & \boldsymbol{0} & \boldsymbol{K}_{4,3}^S & \boldsymbol{K}_{4,4} & \boldsymbol{K}_{4,5}^S & \boldsymbol{0} & \boldsymbol{K}_{4,CT} & \boldsymbol{K}_{4,LS} \\ \boldsymbol{0} & \boldsymbol{0} & \boldsymbol{0} & \boldsymbol{K}_{5,4}^S & \boldsymbol{K}_{5,5} & \boldsymbol{K}_{5,6}^S & \boldsymbol{K}_{5,CT} & \boldsymbol{K}_{5,LS} \\ \boldsymbol{K}_{6,1}^S & \boldsymbol{0} & \boldsymbol{0} & \boldsymbol{0} & \boldsymbol{K}_{6,5}^S & \boldsymbol{K}_{6,6} & \boldsymbol{K}_{6,CT} & \boldsymbol{K}_{6,LS} \\ \boldsymbol{K}_{CT,1} & \boldsymbol{K}_{CT,2} & \boldsymbol{K}_{CT,3} & \boldsymbol{K}_{CT,4} & \boldsymbol{K}_{CT,5} & \boldsymbol{K}_{CT,6} & \boldsymbol{K}_{CT,CT} & \boldsymbol{0} \\ \boldsymbol{K}_{LS,1} & \boldsymbol{K}_{LS,2} & \boldsymbol{K}_{LS,3} & \boldsymbol{K}_{LS,4} & \boldsymbol{K}_{LS,5} & \boldsymbol{K}_{LS,6} & \boldsymbol{0} & \boldsymbol{K}_{LS,LS} \end{bmatrix}, \tag{10}$$

where subscripts separated by comma denote linked FA subsystems.

Each fuel assembly (see Fig. 3) is fixed by means of lower tailpiece (LP) into mounting plate in core barrel bottom and by means of head piece (HP) into lower supporting plate of the block of protection tubes. These support plates with pieces can be considered in transverse direction as rigid bodies.

Let use consider the spatial motion of the support plates described in coordinate systems $x_X, y_X, z_X (X = L, U)$ with origins in plate gravity centres L, U by displacement vectors (see Fig. 7)

$$\boldsymbol{q}_X = [x_X, y_X, z_X, \varphi_{x,X}, \varphi_{y,X}, \varphi_{z,X}]^T,\ X = L, U. \tag{11}$$

The lateral $\xi_{r,X}^{(s)}$, $\eta_{r,X}^{(s)}$ and bending $\vartheta_{r,X}^{(s)}$, $\psi_{r,X}^{(s)}$ displacements in the end-nodes of the fuel rod or guide thimbles r in segment s (in Fig. 7 illustrated for $s = 1$) coupled with plates can

be expressed by the displacements of the lower ($X = L$) and upper ($X = U$) plates (detailed to [5]). The vectors of generalised coordinates of the fully restrained subsystems (rod segments and centre tube) loosed in kinematically excited nodes can be partitioned in the form

$$\boldsymbol{q}_s = [(\boldsymbol{q}_L^{(s)})^T, (\boldsymbol{q}_F^{(s)})^T, (\boldsymbol{q}_U^{(s)})^T]^T,\ s = 1, \ldots, 6, CT \tag{12}$$

and the skeleton $s = LS$ fixed in bottom ends only has the form

$$\boldsymbol{q}_{LS} = [(\boldsymbol{q}_L^{(LS)})^T, (\boldsymbol{q}_F^{(LS)})^T]^T. \tag{13}$$

The displacements of free system nodes (uncoupled with support plates) are integrated in vectors $\boldsymbol{q}_F^{(s)} \in R^{n_s}$. The vibration of the FR excited by pressure pulsations generated by main circulation pumps are described by corresponding components $\xi_{r,g}^{(s)}$, $\eta_{r,g}^{(s)}$, $\vartheta_{r,g}^{(s)}$, $\psi_{r,g}^{(s)}$ of the generalised coordinate vectors $\boldsymbol{q}_F^{(s)}$. Their calculation was presented in [5].

3. The contact forces between fuel rods and spacer grid cells

Consider the inner fuel rod u that is surrounded with six fuel rods $u+1$, v, $v-1$, $u-1$, w, $w+1$ (see Fig. 2) that are uniformly arranged. Their marking correspond to the one applied in the global fuel assembly model. A real contact between fuel rod u and the spacer grid on every one level is realized by three cells $i = 1, 2, 3$. Elastic properties of one cell can be expressed by three springs with identical stiffnesses k.

Let the fuel rod u be loaded by external static force $\vec{F}(F_x, F_y)$ and the centres surrounded fuel rods are fixed. The static displacements x_i, y_i ($i = 1, 2, 3$) of the cell centres and x_u, y_u of the FR u centre in the directions of coordinate axes x, y, due to their flexibility, satisfy the relations

$$\begin{aligned}
F_{u,1} &= k(x_u - x_1),\\
F_{u,2} &= k\left(0.5x_2 - \frac{\sqrt{3}}{2}y_2 - 0.5x_u + \frac{\sqrt{3}}{2}y_u\right),\\
F_{u,3} &= k\left(0.5x_3 + \frac{\sqrt{3}}{2}y_3 - 0.5x_u - \frac{\sqrt{3}}{2}y_u\right),
\end{aligned} \tag{14}$$

where $F_{u,i}$ are contact forces between fuel rod u and cells. From the static equilibrium conditions of each cell we obtain static displacements of their centres

$$\begin{aligned}
x_1 &= \frac{2}{3}x_u; \quad y_1 = 0,\\
x_2 &= \frac{1}{3}\left(0.5x_u - \frac{\sqrt{3}}{2}y_u\right); \quad y_2 = \frac{1}{\sqrt{3}}\left(-0.5x_u + \frac{\sqrt{3}}{2}y_u\right),\\
x_3 &= \frac{1}{3}\left(0.5x_u + \frac{\sqrt{3}}{2}y_u\right); \quad y_2 = \frac{1}{\sqrt{3}}\left(0.5x_u + \frac{\sqrt{3}}{2}y_u\right).
\end{aligned} \tag{15}$$

The deformation energy of all three cells is

$$E_p = \frac{1}{2}k \left[(x_u - x_1)^2 + \left(0.5x_1 + \frac{\sqrt{3}}{2}y_1\right)^2 + \left(0.5x_1 - \frac{\sqrt{3}}{2}y_1\right)^2 + \left(\frac{\sqrt{3}}{2}y_u - 0.5x_u + 0.5x_2 - \frac{\sqrt{3}}{2}y_2\right)^2 + \left(0.5x_2 + \frac{\sqrt{3}}{2}y_2\right)^2 + x_2^2 + \left(0.5x_3 + \frac{\sqrt{3}}{2}y_3 - 0.5x_u - \frac{\sqrt{3}}{2}y_u\right)^2 + x_3^2 + \left(0.5x_3 - \frac{\sqrt{3}}{2}y_3\right)^2 \right]. \tag{16}$$

By elimination of the displacements $x_i,\ y_i$ in term (16) according to (15) we get

$$E_p = \frac{1}{2}0.5k(x_u^2 + y_u^2). \tag{17}$$

The deformation energy of six alternate springs, which represent the elastic properties of couplings between fuel rod u and six surrounding fuel rods in the global fuel assembly model, is

$$E_p = \frac{1}{2}k_g \left[\left(\frac{\sqrt{3}}{2}x_u + 0.5y_u\right)^2 + y_u^2 + \left(-\frac{\sqrt{3}}{2}x_u + 0.5y_u\right)^2 + \left(-\frac{\sqrt{3}}{2}x_u - 0.5y_u\right)^2 + y_u^2 + \left(\frac{\sqrt{3}}{2}x_u - 0.5y_u\right)^2 \right] \tag{18}$$

and after modification

$$E_p = \frac{1}{2}3k_g(x_u^2 + y_u^2). \tag{19}$$

An equality of the right hand sides of the expressions (17) and (19) leads to $k_g = \frac{1}{6}k$ or $k_g = 0.5\,k_b$, where k_b is the cell stiffness defined by

$$k_b = \frac{F_{u,1}}{x_u}. \tag{20}$$

The dynamic contact forces $F_{u,1},\ F_{u,2}$ and $F_{u,3}$ (see Fig. 8) between fuel rod u of segment s and cells at the level spacer grid g (indexes g and s is father let-out) in the course of fuel assembly vibration can be expressed by means of cell centres displacements $x_i,\ y_i\ (i = 1, 2, 3)$ and lateral displacements $\xi_u, \eta_u, \ldots, \xi_{w+1}, \eta_{w+1}$ of six fuel rods surrounding the chosen FR. Fuel rod lateral displacements are generalised displacements of the fuel assembly global mathematical model presented in [5, 7]. These *dynamic contact forces* acting between spacer grid cell 1 and fuel rods $u, u+1$ and $w+1$ can be expressed as

$$\begin{aligned} F_{u,1} &= k\left[-x_1 + \xi_u C(\alpha_u) + \eta_u C\left(\alpha_u + \frac{\pi}{2}\right)\right], \\ F_{u+1,1} &= k\left[0.5x_1 + \frac{\sqrt{3}}{2}y_1 + \xi_{u+1}C\left(\alpha_{u+1} + \frac{2}{3}\pi\right) + \eta_{u+1}C\left(\alpha_{u+1} + \frac{7}{6}\pi\right)\right], \\ F_{w+1,1} &= k\left[0.5x_1 - \frac{\sqrt{3}}{2}y_1 - \xi_{w+1}C\left(\alpha_{w+1} + \frac{1}{3}\pi\right) - \eta_{w+1}C\left(\alpha_{w+1} + \frac{5}{6}\pi\right)\right]. \end{aligned} \tag{21}$$

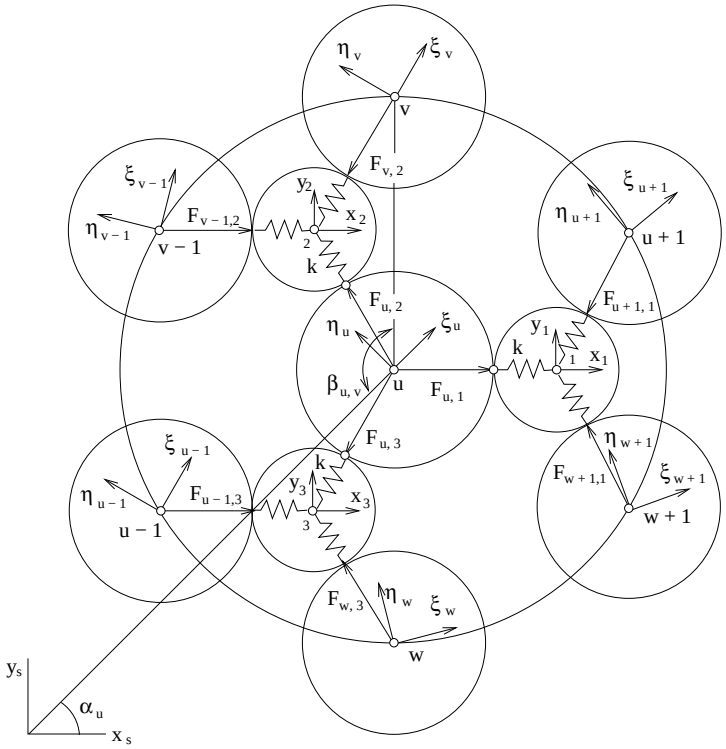

Fig. 8. The contact forces between the fuel rods and the spacer grid cells

The function cosine is shortly marked C with argument in bracket which describes fuel rod angle position in the local coordinate system x_s, y_s of the segment s. The expressions for centre cell lateral displacements follow from the static equilibrium of the considered cell

$$F_{u,1} = F_{u+1,1} = F_{w+1,1}.$$

These displacements can be written as

$$\begin{aligned} x_1 = \frac{1}{3}\Bigg[&2\xi_u C(\alpha_u) + 2\eta_u C\left(\alpha_u + \frac{1}{2}\pi\right) - \xi_{u+1} C\left(\alpha_{u+1} + \frac{2}{3}\pi\right) - \\ &\eta_{u+1} C\left(\alpha_{u+1} + \frac{7}{6}\pi\right) + \xi_{w+1} C\left(\alpha_{w+1} + \frac{1}{3}\pi\right) + \eta_{w+1} C\left(\alpha_{w+1} + \frac{5}{6}\pi\right)\Bigg], \\ y_1 = \frac{1}{\sqrt{3}}\Bigg[&-\xi_{u+1} C\left(\alpha_{u+1} + \frac{2}{3}\pi\right) - \eta_{u+1} C\left(\alpha_{u+1} + \frac{7}{6}\pi\right) - \\ &\xi_{w+1} C\left(\alpha_{w+1} + \frac{1}{3}\pi\right) - \eta_{w+1} C\left(\alpha_{w+1} + \frac{5}{6}\pi\right)\Bigg]. \end{aligned} \tag{22}$$

In a similar way we derive centre cell lateral displacements of other cells 2 and 3

$$\begin{aligned} x_2 = \frac{1}{3}\Bigg[&2\xi_{v-1} C(\alpha_{v-1}) + 2\eta_{v-1} C\left(\alpha_{v-1} + \frac{1}{2}\pi\right) + \xi_u C\left(\alpha_u + \frac{1}{3}\pi\right) + \\ &\eta_u C\left(\alpha_u + \frac{5}{6}\pi\right) + \xi_v C\left(\alpha_v - \frac{1}{3}\pi\right) + \eta_v C\left(\alpha_v + \frac{1}{6}\pi\right)\Bigg], \\ y_2 = \frac{1}{\sqrt{3}}\Bigg[&\xi_v C\left(\alpha_v - \frac{1}{3}\pi\right) + \eta_v C\left(\alpha_v + \frac{1}{6}\pi\right) - \\ &\xi_u C\left(\alpha_u + \frac{1}{3}\pi\right) - \eta_u C\left(\alpha_u + \frac{5}{6}\pi\right)\Bigg], \end{aligned} \tag{23}$$

$$x_3 = \frac{1}{3}\left[2\xi_{u-1}C(\alpha_{u-1}) + 2\eta_{u-1}C\left(\alpha_{u-1}+\frac{1}{2}\pi\right) - \xi_u C\left(\alpha_u+\frac{2}{3}\pi\right) - \eta_u C\left(\alpha_u+\frac{7}{6}\pi\right) + \xi_w C\left(\alpha_w+\frac{1}{3}\pi\right) + \eta_w C\left(\alpha_w+\frac{5}{6}\pi\right)\right], \tag{24}$$

$$y_3 = \frac{1}{\sqrt{3}}\left[-\xi_u C\left(\alpha_u+\frac{2}{3}\pi\right) - \eta_u C\left(\alpha_u+\frac{7}{6}\pi\right) - \xi_w C\left(\alpha_w+\frac{1}{3}\pi\right) - \eta_w C\left(\alpha_w+\frac{5}{6}\pi\right)\right].$$

The *total contact forces* between fuel rod u in the segment $s = 1, \ldots, 6$ and the spacer grid cells at the level $g = 1, \ldots, G$ (indexes s and g are let-out) are determined by the sum of the static contact force F_{st} after fuel rods installation into the load-bearing skeleton with spacer grids and the dynamic contact forces caused by vibration

$$N_{u,i}(t) = [F_{st} + F_{u,i}(t)]H(F_{st} + F_{u,i}(t)),\ i = 1, 2, 3. \tag{25}$$

H is Heaviside function (for $F_{st} + F_{u,i}(t) < 0$, when contact is interrupted, $H = 0$). The dynamic contact forces of the fuel rod u with cells are expressed in the form (see Fig. 8)

$$F_{u,1} = k\left[-x_1 + \xi_u C(\alpha_u) + \eta_u C\left(\alpha_u+\frac{1}{2}\pi\right)\right],$$
$$F_{u,2} = k\left[0.5x_2 - \frac{\sqrt{3}}{2}y_2 - \xi_u C\left(\alpha_u+\frac{1}{3}\pi\right) - \eta_u C\left(\alpha_u+\frac{5}{6}\pi\right)\right], \tag{26}$$
$$F_{u,3} = k\left[0.5x_3 + \frac{\sqrt{3}}{2}y_3 + \xi_u C\left(\alpha_u+\frac{2}{3}\pi\right) + \eta_u C\left(\alpha_u+\frac{7}{6}\pi\right)\right],$$

where k is the stiffness of the one substitute spring of the cell. Substituting the expressions (22), (23), (24) of the centre cell lateral displacements into force equations (26), we obtain dynamic contact forces occuring in Eq. (25). The fuel rod u angle position in each segment after its installation is determined by polar coordinate α_u (see Fig. 6).

4. The power and the work of the friction forces in the contact of fuel rods coating with the spacer grid cell

The *slip speeds* between the transfer vibrating spacer grid on the level g and the fuel rod u in segment s due to the fuel rod bending inside of the spacer grid cell in contact points C_i, $i = 1, 2, 3$ (see Fig. 9) are

$$c_{u,1} = r\left[\sin\left(\frac{1}{2}\pi - \beta_{u,v}\right)\dot{\vartheta}_u - \cos\left(\frac{1}{2}\pi - \beta_{u,v}\right)\dot{\psi}_u\right],$$
$$c_{u,2} = r\left[\sin\left(\frac{7}{6}\pi - \beta_{u,v}\right)\dot{\vartheta}_u - \cos\left(\frac{7}{6}\pi - \beta_{u,v}\right)\dot{\psi}_u\right], \tag{27}$$
$$c_{u,3} = r\left[\sin\left(\frac{11}{6}\pi - \beta_{u,v}\right)\dot{\vartheta}_u - \cos\left(\frac{11}{6}\pi - \beta_{u,v}\right)\dot{\psi}_u\right],$$

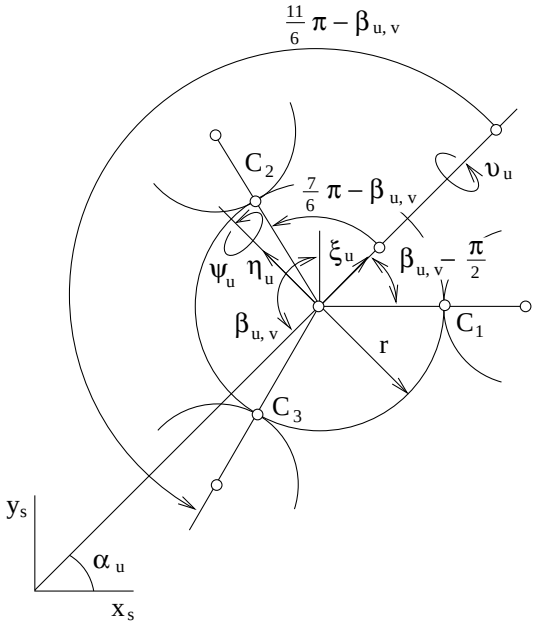

Fig. 9. The contact point positions of the fuel rod u with the spacer grid cells

where r is outside diameter of the fuel rod coating. Bending angular velocities of the fuel rod cross-sections are expressed by corresponding components of the vector $\dot{\boldsymbol{q}}_F^{(s)}(t)$ obtained by the derivative with respect to time of the generalised coordinate vector $\boldsymbol{q}_F^{(s)}$ of the fuel assembly free node displacements defined in (12). The *power of the friction forces* in the contact points C_j of the fuel rod u coating in segment s and the spacer grid cells on the level g is

$$P_{u,i}(t) = f_0 N_{u,i}(t) c_{u,i}(t), \quad i = 1, 2, 3, \tag{28}$$

where f_0 is computational friction coefficient. The criterion of the fuel rod coating abrasion can be expressed by the *work of the friction forces* during the period T [s] of the first harmonic component of pressure pulsations

$$W_{u,i} = \int_0^T |P_{u,i}(t)| \, \mathrm{d}t. \tag{29}$$

On the basis of experimental investigated friction coefficient $f(T)$ and mass loss μ [gJ^{-1}] in grams [4] of the fuel rod coating caused by the work of the friction force $W = 1$ [J] we can calculate the fuel rod coating abrasion in the contact line segment during the operational period t_p [s]

$$\Delta m_i = \mu W_{u,i} \cdot \frac{f(T)}{f_0} \cdot \frac{t_p}{T} \, [\mathrm{g}], \quad i = 1, 2, 3. \tag{30}$$

5. Application

The presented methodology was applied for steady polyharmonic dynamic response of the Russian TVSA-T fuel assembly in the WWER 1000/320 type reactor core in NPP Temelín. Mathematical model of the WWER 1000/320 type reactor excited by pressure pulsations was derived in [6] by the decomposition method presented in [8]. The linearized model has the standard form

$$\boldsymbol{M}\ddot{\boldsymbol{q}}(t) + \boldsymbol{B}\dot{\boldsymbol{q}}(t) + \boldsymbol{K}\boldsymbol{q}(t) = \boldsymbol{f}(t), \tag{31}$$

where the vector of generalised coordinates of dimension 137 is specified in [6].

The reactor is a large multi-body system which includes no special dampers. The first approximation of the damping consists in assuming that the system is lightly damped and that the damping matrix $\boldsymbol{B}$ satisfies the general condition of proportional damping in the form $\boldsymbol{V}^T\boldsymbol{B}\boldsymbol{V} = \mathrm{diag}\,[2D_\nu\Omega_\nu]$, where $\boldsymbol{V} = [\boldsymbol{v}_\nu]$ is modal matrix of the reactor conservative model. Its eigenfrequencies are noted Ω_ν and eigenvectors $\boldsymbol{v}_\nu$ satisfying the norm

$$\boldsymbol{v}_\nu^T\boldsymbol{M}\boldsymbol{v}_\nu = 1, \quad \nu = 1, \ldots, 137.$$

The dimensionless damping factors D_ν were considered, on the basis of experience in modelling of nuclear reactor vibrations, equal 0.05 with the exception of the damping factors corresponding to eigenmodes, where the reactor core dominantly vibrates. In consequence of an influence of coolant these factors were considered larger, concretely $D_\nu = 0.08$. After an estimation of all damping factors the damping matrix in the mathematical model (31) is calculated as

$$\boldsymbol{B} = (\boldsymbol{V}^{-1})^T\mathrm{diag}\,[2D_\nu\Omega_\nu]\boldsymbol{V}^{-1}.$$

The excitation vector $\boldsymbol{f}(t)$ can be written as a real part of the complex excitation vector

$$\boldsymbol{f}(t) = \mathrm{Re}\left[\sum_j\sum_k \boldsymbol{f}_j^{(k)}\mathrm{e}^{\mathrm{i}k\omega_j t}\right], \quad j = 1, 2, 3, 4, \tag{32}$$

where $\boldsymbol{f}_j^{(k)}$ is vector of complex amplitudes of k-th harmonic component of the hydrodynamic force generated by one j-th main circulation pump. The fluctuation of the main circulation pump angular speeds $\omega_j = \pi\frac{n_j}{30}$, $n_j \in \langle 997.2, 999.6\rangle$ [rpm] is based on the measurement at the first and second NPP Temelín blocks [6].

The steady-state dynamic response of the reactor is given by the particular solution

$$\boldsymbol{q}(t) = \mathrm{Re}\left\{\sum_j\sum_k \left[-(k\omega_j)^2\boldsymbol{M} + \mathrm{i}k\omega_j\boldsymbol{B} + \boldsymbol{K}\right]^{-1}\boldsymbol{f}_j^{(k)}\mathrm{e}^{\mathrm{i}k\omega_j t}\right\}. \tag{33}$$

The generalised coordinates in dependence on time can be written in the form

$$q_i(t) = \sum_j\sum_k \left(\overline{q}_{i,j}^{(k)}\cos k\omega_j t - \overline{\overline{q}}_{i,j}^{(k)}\sin k\omega_j t\right), \tag{34}$$

where real (with one strip) and imaginary (with two strips) components of complex vector

$$\boldsymbol{q}_j^{(k)} = \left[-(k\omega_j)^2\boldsymbol{M} + \mathrm{i}k\omega_j\boldsymbol{B} + \boldsymbol{K}\right]^{-1}\boldsymbol{f}_j^{(k)} \tag{35}$$

are introduced. Subscript $i = 1, \ldots, 137$ is assigned to the generalised coordinate, subscript $j = 1, 2, 3, 4$ to the operating main circulation pumps and subscript k to the harmonic component of pressure pulsations. The components of the vectors $\boldsymbol{q}_j^{(k)}$, corresponding to displacements of the lower fuel assembly supporting plate in the lower part of core barrel (CB3) depicted in Fig. 4 and the upper fuel assembly supporting plate (SP) in the block of protection tubes (BPT), are transformed into displacement vector $\boldsymbol{q}_X$ defined in (11) and next into lateral and bending displacements in the end-nodes of the subsystem components [5].

As an illustration, extreme values of the total contact forces $F_{u,i}$, vertical slip displacements $y_{u,i}$ and speeds $c_{u,i}$ of the fuel rod coating in contact points C_i, power $P_{u,i}^{(s)}$ and work $W_{u,i}^{(s)}$ of

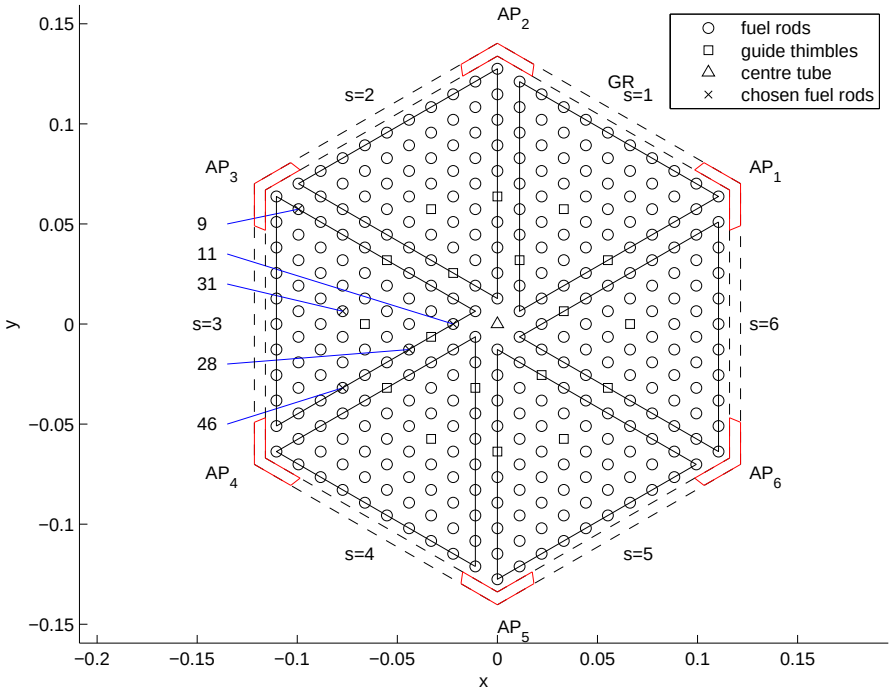

Fig. 10. The fuel assembly cross-section with chosen rods

Table 1. Extreme values at contact points of the fuel rod u in segment $s = 3$ with spacer grid cells on the level $g = 1$

Quantity	units	mark	Extreme values				
			$u = 9$	$u = 11$	$u = 28$	$u = 31$	$u = 46$
FR contact forces vs. cells	N	$F_{u,1}$	29.0	20.7	21.8	20.9	22.6
		$F_{u,2}$	20.7	21.3	21.5	20.5	21.1
		$F_{u,3}$	24.2	21.1	22.1	20.7	21.1
FR slip displacements vs. cells	μm	$y_{u,1}$	5.98	6.53	6.94	6.12	6.56
		$y_{u,2}$	7.54	8.34	8.64	7.71	7.92
		$y_{u,3}$	2.98	2.98	3.39	2.91	3.48
FR slip speeds PP vs. cells	mm/s	$c_{u,1}$	1.15	1.02	1.04	1.00	1.00
		$c_{u,2}$	1.53	1.46	1.38	1.26	1.18
		$c_{u,3}$	0.47	0.54	0.57	0.48	0.56
Friction power in contact points	mW	$P_{u,1}$	5.35	4.07	4.15	4.01	4.00
		$P_{u,2}$	6.08	5.92	5.66	4.98	4.73
		$P_{u,3}$	1.91	2.13	2.42	1.92	2.24
Friction work in contact points	μJ	$W_{u,1}$	123	96.0	104	98.1	102
		$W_{u,2}$	164	131	134	122	121
		$W_{u,3}$	50.8	49.2	53.5	46.8	54.0

the friction forces for chosen fuel rods $u = 9, 11, 28, 31, 46$ (see Fig. 10) in segment $s = 3$ on the level of spacer grid $g = 1$ are demonstrated in Table 1.

The time behaviour of these quantities for spacer grid cells surrounding the fuel rod $u = 46$, with the exception of work, in time interval $t \in \langle 0; 100 \rangle$ [s] are shown in Figs. 11–14. This time interval of the numerical simulation includes the long period $\frac{60}{\Delta n}$ [s] of the beating vibrations caused by slightly different main circulation pumps revolutions Δn [rpm].

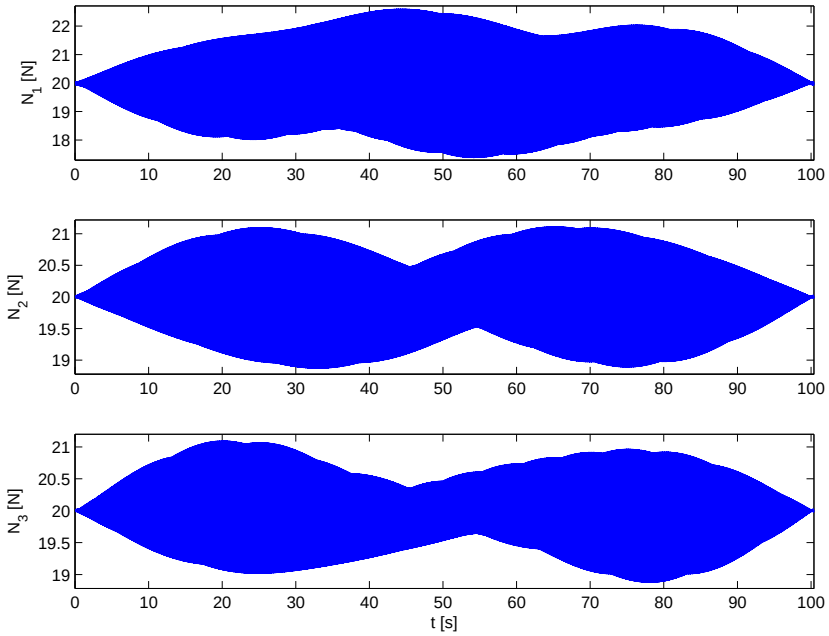

Fig. 11. The contact forces between fuel rod $u = 46$ in segment $s = 3$ and spacer grid cells on the level $g = 1$

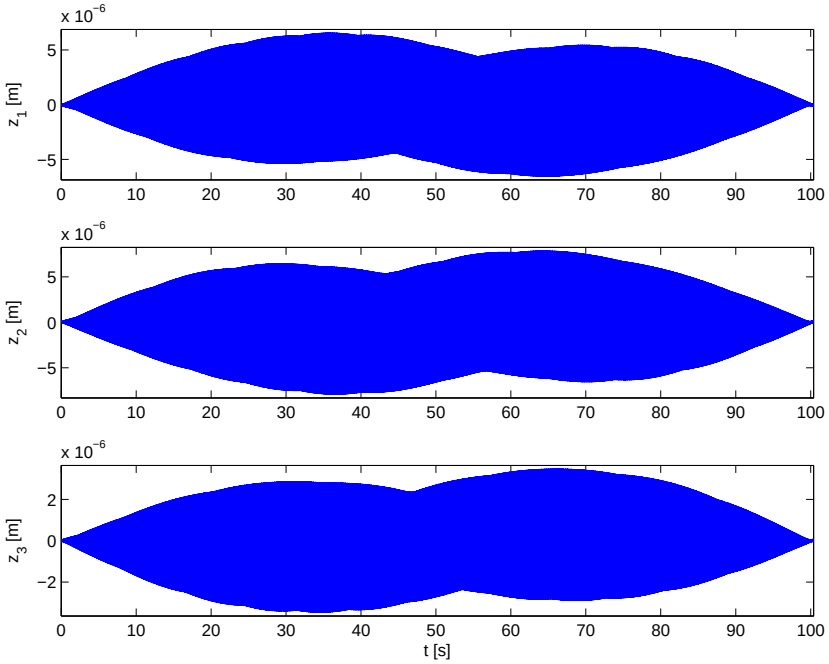

Fig. 12. The vertical slip displacements between fuel rod $u = 46$ in segment $s = 3$ and spacer grid cells on the level $g = 1$

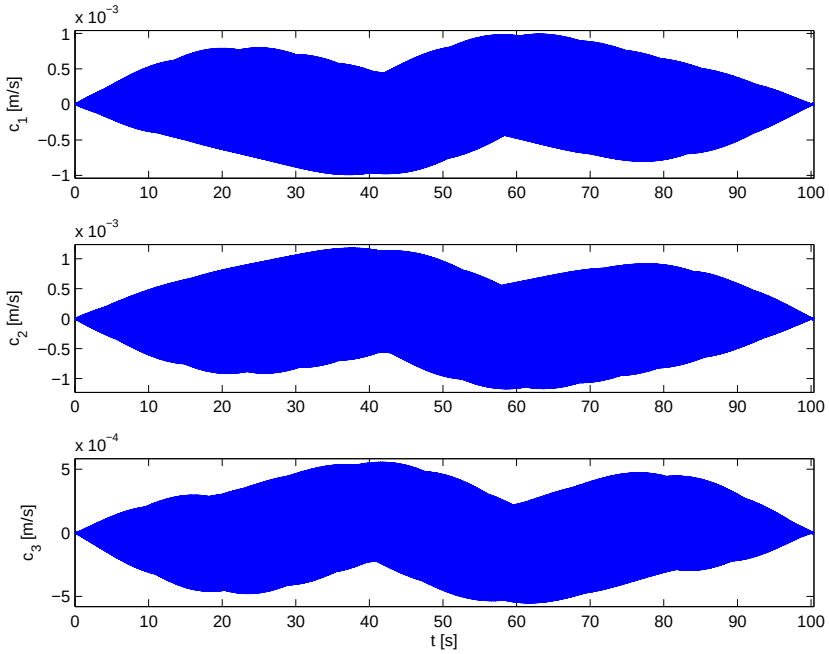

Fig. 13. The vertical slip speeds between fuel rod $u = 46$ in segment $s = 3$ and spacer grid cells on the level $g = 1$

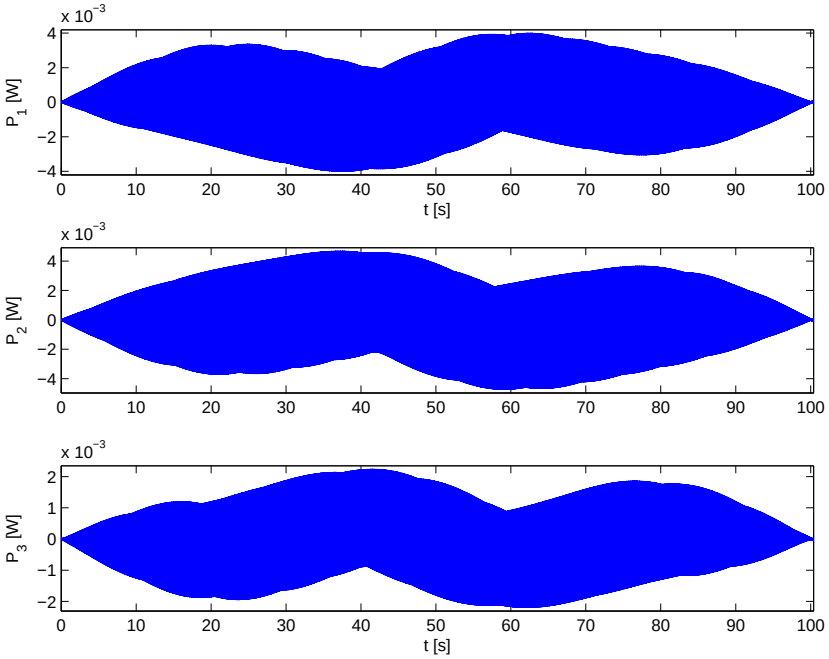

Fig. 14. The power of the friction forces between fuel rod $u = 46$ in segment $s = 3$ and spacer grid cells on the level $g = 1$

6. Conclusion

The described method enables to investigate the flexural kinematically excited vibrations of all fuel assembly components. The vibrations are caused by spatial motion of the two horizontal supporting plates in the reactor core transformed into displacements of the kinematically excited nodes of the fuel assembly components — fuel rods, guide thimbles, centre tube and skeleton angle pieces. The special coordinate system of radial and orthogonal lateral and flexural angular displacements around these directions of the fuel rods and guide thimbles enables to separate the hexagonal type FA into six identical revolved rod segments characterized in global fuel assembly mathematical model by identical mass, damping and stiffness matrices. These identical subsystems are linked each other and with centre tube and skeleton by spacer grids on the several level. The elastic properties of the spacer grid on the different horizontal levels g are expressed in the fuel assembly global model by alternate springs with stiffnesses k_g calculated on the basis of their identical deformation energy with cells. All fuel assembly components are modelled as one dimensional continuum of beam type with nodal points in the gravity centres of their cross-sections on the level of the spacer grids.

The developed methodology was used for steady-state vibration analysis of the Russian type nuclear fuel assembly caused by motion of the support plates, excited by pressure pulsations generated by main circulation pumps in the coolant loops of the primary circuit. The developed software in MATLAB is conceived in such a way that enables to choose an arbitrary configuration of operating pumps whose rotational frequencies are slightly different in the experimentally determined frequency interval $f \in \langle 16.635; 16.645 \rangle$ Hz. This phenomenon results in beat vibrations, which amplify dynamic normal and friction forces in the contact of the fuel rod coating and spacer grid cells. The software enables an identification of the maximal dynamic loaded spacer grid cell and calculation of the maximal normal contact forces between fuel rod coating and surrounding spacer grid cells for the arbitrary fuel rod on the arbitrary spacer grid levels. Subsequently we can calculate the friction force work in the contact lines of the chosen fuel rod with cells during defined time period. In this way the abrasion of fuel rod coating can be estimated.

Acknowledgements

This work was supported by the European Regional Development Fund (ERDF), project "NTIS", European Centre of Excellence, CZ.1.05/1.1.00/02.0090 within the research project "Fuel cycle of NPP" of the NRI Řež plc.

References

[1] Fuel Assembly Mechanical Test Report, volume I a II, TEM-MC-04.RP (Rev 0), Property of JSC "TVEL", NRI Řež, 2011.

[2] Jeník, J., Mechanical model for cell stiffness determination of the TVSA-T fuel assembly. Research report Ae 14 947/Dok, Škoda JS, a. s., 2013 (in Czech).

[3] Pečínka, L., Stulík, P., The Experimental Verification of the Reactor WWER 1000/320 Dynamic Response Caused by Pressure Pulsations Generated by Main Circulation Pumps. In: Proceedings of Colloquium Dynamics of Machines 2008, ed. L. Pešek, Institute of Thermomechanics AS CR, Prague (2008), pp. 87–94.

[4] Svoboda, J., Šmíd, Z., Klášterka, P., Study of the influence of selected factors on the abrasion of components made of ZR material. Research report Z-1497/13, Institute of Thermomechanics, Academy of Sciences of the Czech Republic v.v.i, Pilsen, 2013 (in Czech).

[5] Zeman, V., Hlaváč, Z., Dynamic response of nuclear fuel assembly excited by pressure pulsations. Applied and Computational Mechanics 6(2) (2012) 219–230.

[6] Zeman, V., Hlaváč, Z., Dynamic response of VVER 1000 type reactor excited by pressure pulsations. Engineering Mechanics 15(6) (2008) 435–446.

[7] Zeman, V., Hlaváč, Z., Modelling and modal properties of the nuclear fuel assembly. Applied and Computational Mechanics 5(2) (2011) 253–266.

[8] Zeman, V., Hlaváč, Z., Modelling of WWER 1000 type reactor vibration by means of decomposition method. In: Engineering Mechanics 2006, Book of extended abstracts, ed. J. Náprstek and C. Fischer, Institute of Theoretical and Applied Mechanics AS CR, Prague (2006), pp. 444–445 (full text on CD-ROM) (in Czech).